Bone microarchitecture in human fetuses

Françoise Peyrin[1,2]
Georges Boivin[3]
Pierre Braillon[4]

[1] CREATIS, CNRS UMR 5515, Inserm U630, 69621 Villeurbanne Cedex, France
[2] ESRF, BP 220, 38043 Grenoble Cedex, France
[3] Inserm U403, 69372 Lyon Cedex 08, France
[4] Hôpital Debrousse, Dpt of Pediatric Imaging, 69322 Lyon Cedex 05, France

Address for correspondence:
Françoise Peyrin, Ph.D.
ESRF, BP 220, 38043 Grenoble Cedex, France
Ph. +33 4 76 88 23 35
Fax +33 4 76 88 22 52
E-mail: peyrin@esrf.fr

Summary

Bone microarchitecture is receiving increasing attention in the assessment of the biomechanical properties of bone. While it is well characterized in normal and pathologic human subjects, few quantitative data are available in human fetal development. In this paper, quantitative parameters of bone microarchitecture in developing human bone are reviewed from the literature and supplemented by new data from the femoral metaphysis of human fetuses. The samples were imaged using synchrotron radiation 3D micro-CT and processed using customized analysis methods. This technique provides 3D model independent morphometric parameters anisotropy, connectivity and geometry characteristics, as well as information on mineralization.
The morphometric parameters obtained on fetal vertebrae and femurs evidenced a dense trabecular structure as compared to that of young adults. The histomorphometric and the 3D micro-CT analysis were consistent to show a significant increase of trabecular bone volume with gestational age. Trabecular bone was found isotropic in vertebral bodies and anisotropic in femoral metaphysis, demonstrating a radial growth in vertebrae, and a longitudinal spreading out in long bones such as the femurs. Trabecular thickness in the mature bone of vertebral body and femoral metaphysis was around 100 µm, which was in agreement with histomorphometric evaluation. In the femoral metaphysis, three-dimensional analysis confirmed the thickening of trabeculae with the distance to the growth plate, and an estimated rate of thickening around 3 µm/day previously obtained in histomorphometry. The 3D network was highly connected, and our new geometrical analysis technique showed a strong prevalence of rod structure as compared to the plate structure in cancellous bone.

KEY WORDS: bone microarchitecture, fetus, micro-CT, three-dimensional imaging, development.

Introduction

Bone microarchitecture is receiving increasing attention in the assessment of the biomechanical properties of bone. If it is well characterized in normal and pathologic human subjects, few quantitative data are available in human fetal development. The different stages of bone formation in human embryo have been extensively described in histological textbooks (1-3). Ossification begins as mesenchymal condensations during the embryonic period. Bone formation is typically classified in intramembranous and endochondral ossification. In intramembranous (or dermal) ossification, the mesenchymal tissue is directly converted into bone, while in endochondral ossification, the mesenchymal cells differentiate into a cartilage model, which is later replaced by bone. Intramembranous ossification concerns flat bones of the skull and face, the mandible and the clavicle. Endochondral ossification concerns most bone of the skeleton, and in particular bones of the axial skeleton and long bones.

Endochondral ossification involves several steps (2):

1) Chondrocytes in the centre of the cartilage model hypertrophy. The matrix is reduced to a series of small struts that soon begin to calcify. After they initiate matrix changes, the enlarged chondrocytes degenerate and disintegrate leaving cavities within cartilage.
2) Blood vessels grow into the perichondrium surrounding the shaft of the cartilage. The cells in the inner layer of the perichondrium differentiate into osteoblasts. The perichondrium is now a periosteum, and a thin layer of bone is produced around the shaft of the cartilage.
3) Blood invasion increases by capillaries penetrating in the space left by the disintegrating chondrocytes. Osteoblasts begins producing spongy bone. This primary center of ossification expands towards both ends of the cartilage model.
4) As the bone enlarges, trabeculae in the center of the shaft region are resorbed and form a marrow cavity. The bone of the shaft becomes thicker and the cartilage between each epiphyses is replaced by shafts of bone. Further growth involves increase in length and diameter.
5) Capillaries and osteoblasts migrate into the epiphyses creating secondary ossification centers. The epiphyses become filled with spongy bone. At each metaphysis an epiphyseal cartilage separates the epiphyses from the diaphysis.

The initial site of bone deposition, called a primary ossification center, appears in human fetus from the 8th week of gestation (4). Later on, secondary ossification centers occur for instance in the epiphyses of long bone. The first bone tissue formed in the embryo is an immature bone, called woven bone or nonlamellar bone. Woven bone can be formed very rapidly and may also be found in adults when bone has been remodeled or in fracture healing. In this tissue, the collagen fibers of the matrix are arranged irregularly in the form of a meshwork. Woven bone is gradually converted to lamellar bone. Woven bone may be recognized from mature bone by appropriate staining in histology.

At the cell levels, osteoblasts and osteoclasts are respectively responsible for bone deposition or bone removal. Another type of cells, osteocytes, which are osteoblasts that have been trapped in bone matrix during tissue production, communicate through a network of canaliculi and serve as sensors of mechanical stimuli within bone tissue. Bone growth involves rapid changes in shape and in size. The dynamic of bone activity

may be described by bone modeling or remodeling. The cellular interactions associated with remodeling cycles follow a sequence of four main stages, activation, resorption, reversal and formation, well described by Parfitt (5). In bone remodeling the activity of osteoblasts and osteoclasts is coupled, bone resorption and formation occurring at the same locations on bone surfaces. After a remodeling cycle, bone mass is preserved in normal young adult bone and tends to decline with aging. In contrast, during bone modeling, the activity of osteoblasts and osteoclasts is not coupled, formation and resorption occurring on different surfaces (6, 7). In the growing fetus, modeling is supposed to be the main mechanism governing the rapid changes in bone mass and structure.

Bone formation involves a number of chemical, cellular and morphological processes, the investigation of which requires various techniques at different scales. From a chronologic point of view, histology using light microscopy has been the main technique used to describe the different stages in bone growth and the cellular mechanism involved in bone formation. Histology with appropriate staining enables the appreciation of different type of bones (woven bone, lamellar bone, calcified cartilage...) and examinations at the cell level. The characterization of the crystalline structure and the chemical composition of bone tissue requires techniques at the chemical level, such as x-ray diffraction, electron or infrared microscopy, and infrared or NMR spectroscopy. In (8), the ultrastructure of the initial stages of ossification in human embryos has been studied by light microscopy and scanning electron microscopy. In long bones, matrix vesicles were found amongst maturing and hypertrophic chondrocytes already by the 6th week of gestation. Mineralization of cartilage in long bone started in the form of hydroxyapatite (HAP) crystals within or around the matrix vesicles. The calcification rate in lumbar vertebrae in fetuses aged 17-41 weeks has been documented in (9). However most studies concerning the structural composition and the maturation of early calcium phosphate are still investigated and mostly *in vitro* or on animal models (10-13).

Nowadays, various modalities of medical imaging allow to get insight into bone formation. X-ray radiography (14, 15), and Dual Energy X-ray Absorptiometry (16, 17), relying on the attenuation properties of bone, were used to sequence the ossification centers and evaluate bone mineral density. Quantitative Computed Tomography (QCT) allowed to study the mineral density in developing vertebral bodies, showing an increase of bone mineral density with gestational age (18). However due to x-ray dose limitation, QCT cannot be used to image bone formation *in vivo*. In contrast, ultrasonic imaging methods which are non invasive are well adapted to the follow up of fetus development *in vivo* (19-21). The improvement in the quality of echographic examinations allows to use this technique to control the normality of fetuses. In particular the length of various bone may be measured from ultrasound and normal reference plots of growth are now available (22, 23). Unfortunately, these techniques do not provide information on bone microarchitecture *in vivo*.

Quantitative data of bone microarchitecture during development are thus limited to *ex-vivo* analysis on *post-mortem* bodies and are relatively scarce due to ethical and legal reasons. Histomorphometry was used to assess trabecular microarchitecture in iliac crest bone to investigate osteopenia in preterm neonate (24). The development of the femoral metaphysis has been quantitatively reported in two major papers by the groups of Salle and Glorieux (25, 26). These data are relatively unique in the literature and constitute a reference for architectural parameters in growing human femurs. More recently three-dimensional microtomography (micro-CT) has been used for the evaluation of trabecular bone microarchitecture in human fetal vertebral bodies (27). Micro-CT was recently used to study vascular invasion during the development of the secondary centres of ossification in a rabbit model but no quantification was provided (28).

In the second section, we shall particularly recall the quantification of bone microarchitecture based on 3D micro-CT and review the differences with respect to histomorphometry. In the third section, the results available for the femoral metaphysis and vertebral body bone microarchitecure will be reported. New data obtained from 3D quantitative analysis of micro-CT images on human femurs during gestation will be presented. Finally, the different results will be summarized and discussed in a last section.

Investigation of bone microarchitecture

Imaging techniques

The reference technique for the investigation of bone microarchitecture has for long been histomorphometry, which consists in analyzing histological slices. The bone sample has to be embedded in a resina and a slice with a thickness of a few micrometer is cut. This slice is then examined under a light microscope, and processed using specific quantification methods as described in the next section. However, since the last decade, quantification based on x-ray microtomography (micro-CT) has considerably increased due to the amazing progresses made by this technique, and the availability of commercial systems.

Micro-CT is a high resolution version of CT, used in clinical routine at the hospital. Its principle is to measure the attenuation of x-rays in a slice (or a volume) under different angles of view; then these measures are numerically processed to reconstruct a digital image (or volume). Conversely to histomorphometry which requires the cutting of the bone sample to be analyzed, micro-CT is a non destructive technique requiring no special preparation for the sample. In addition, micro-CT may provide three-dimensional images that are difficult to obtain by using serial histological slices due to slice deformations or deteriorations during cutting. The quantification of bone morphometry may then be directly performed from three-dimensional images, which presents some advantages over bi-dimensional analysis, as will be highlighted in the next section.

Though the accuracy of quantitative microarchitecture parameters is strongly related to image quality in terms of spatial resolution and signal to noise ratio. Spatial resolution refers to the size of the smallest detail that can be observed in the image. It is admitted that for the analysis of adult human trabecular bone a spatial resolution of 10-15 µm is sufficient to get accurate quantification. Spatial resolution is not necessarily equal to the pixel (picture element) size in the image, although there is often some confusion in these terms. The signal to noise ratio in the micro-CT image is another important parameter with respect to the quantification accuracy since a noisy image makes it difficult the separation of bone from background. However, this segmentation is crucial since it is the first step of quantification and strongly influences the subsequent measurements. Keeping the same signal to noise ratio when spatial resolution increases is a technical difficulty to which micro-CT is confronted. A solution to get high signal to noise ratio in limited acquisition time, is to use x-rays with high photon fluxes. X-rays with such characteristics may be produced by synchrotron sources, and synchrotron radiation (SR) micro-CT systems have been developed in a few synchrotron facilities in the world.

A SR micro-CT system has been developed on beam-line ID19 at the ESRF (European Synchrotron Radiation Facility). The system provides three-dimensional images with spatial resolu-

tion between 15 and 0.5 µm, this last resolution being still unachieved by micro-CT systems based on standard x-ray sources. The system has been used for the quantification of bone microarchitecture in human adults (29), animal models (30) and human fetal bone (31). A significant advantage of this system over standard micro-CT is that it enables the simultaneous quantification of bone microarchitecture and tissue mineralization (32), which is possible thanks to the use of monochromatic x-ray beams with sufficient photon fluxes.

Quantification of bone microarchitecture

The nomenclature used for quantifying bone microarchitecture in trabecular or cortical bone has been standardized in a reference paper of Parfitt (33). In order to infer three-dimensional parameters of bone organization from bi-dimensional slices (provided by histology), geometric assumptions on the organization of bone have to be hypothesized. Usually the bone network is supposed to be organized in a parallel plate model (Parfitt's model) (34). Under this assumption, stereology-derived methods allow estimating a number of morphometric parameters from two measures: the percentage of trabecular bone in the sample (Pp) and the normalized number of intersections of bone with a set of regularly spaced parallel test lines measured for various orientations (Pl). The following parameters may then be calculated: Trabecular Bone Volume fraction (BV/TV, where TV stands for total bone sample volume), Bone Surface on Bone Volume ratio (BS/BV), Trabecular Thickness (Tb.Th), Trabecular Number (Tb.N), and Trabecular Separation (Tb.Sp). These parameters are typically computed by using the MIL (Mean Intercept Length) method, which was initially proposed for 2D images, and later generalized to 3D images. In this case, the same relationships are used but the test lines are considered in the whole 3D space (35). Such a method may be applied for the quantification of three-dimensional images provided by micro-CT.
However the so-called-derived architectural parameters have the drawback to rely on a geometrical model of bone structures which is obviously not completely appropriate in all situations. Fortunately this model is no more necessary when three-dimensional images are available. A direct or model-independent method requiring no prior assumption has been proposed to calculate trabecular thickness (36). A theoretical local thickness is defined at each point of the volume as the diameter of the maximal sphere including that point. Similarly, all microarchitectural parameters may be obtained via model-independent methods when using 3D images. The parameters are denoted with a star (for instance Tb.Th*) so as to differentiate them from their standard homonyms.
We proposed a method for computing the local thickness of 3D discrete images based on discrete geometry (37). A medial axis of the bone structure, defined as the center of maximal balls, is derived from the local maxima of a 3D discrete distance map. The discrete thickness map is then obtained by propagating the sorted values of the diameter of the maximal balls to the entire balls. We typically use a 3D Chanfrein distance which provides a good approximation of the Euclidian distance (38). This method provides a thickness value at each point of the bone volume, and thus makes available the distribution of thickness over the entire volume. Statistical results such as the histogram of thickness, and the mean, median, and standard deviation of the distribution are computed.
Three-dimensional images may also be used to get information on the orientation and anisotropy of the structure, as well as on the topology of the bone network (37). Orientation and anisotropy may be obtained from the MIL method by fitting the points defined by each direction and the normalized number of intersections in this direction, by an ellipsoid in 3D space. The degree of anisotropy (DA) is estimated by the ratio of the largest to the smallest axis value. The main orientation of the ellipsoid gives an estimate of the orientation of the structure. Topologic parameters include the Euler number, used to quantify the connectivity of the network, or other characteristics calculated from skeletons like the number of branches, number of connections…
Finally, the global geometry of bone structure in term of plate-like or rod-like model may be estimated globally by the SMI (Structure Model Index) (39). We recently proposed new geometrical indices based on a local classification of bone structures to describe more accurately the percentage of plate and rod volumes (40). The technique is based on an original idea of making a local topological analysis in the neighborhood of each point in order to classify the voxels of the bone structure (40). We used this classification to label four types of points: boundary, branch, plate and rod points. This initial classification is then re-labeled by re-affecting the boundary type which is not relevant to that of their closest neighbors. After this step, the 3-classes labeled image is used for counting the percentage of branch, plate and rod points in the bone volume, that we respectively denote NV/BV, PV/BV, and RV/BV.

Quantification of fetal bone microarchitecture in femurs and vertebal body

Results from histomorphometry

Before reporting microarchitectural parameters on femurs, we recall the evolution of femur size during gestation. Femur lengths at different gestational ages are relatively well known, since they can be examined *in vivo* using obstetrical echography (22, 23). Various formulas relating gestational age from femur lengths have been proposed and are used to evaluate gestational age. Among those we report, the predication proposed by Doubilet (23), which reduces the mean errors to less than 0.6 week in the 14 to 42 weeks period. The relationship between gestational age (GA) and femur length (L) is based on logarithmic regression, $GA = \exp(\alpha + \beta L)$ with $\alpha = 2.45132$, and $\beta = 0.016590$. The variation of femur length as a function of the gestational age, obtained by inverting this formula is illustrated in Figure 1. The dots indicate the characteristics of the femur samples that will be presented in the next section.
We report here quantitative results obtained from the works of

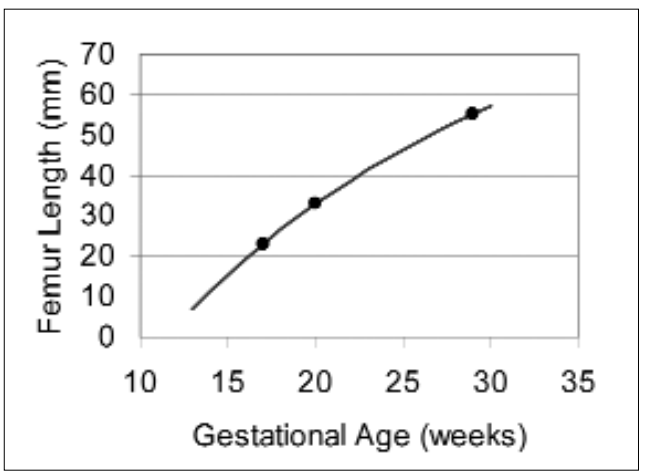

Figure 1 - Evolution of femur length with gestational ages. The dots correspond to the age of femurs examined in section III.2.

Salle, Glorieux et al. (25, 26). Histomorphometry was performed on a collection of samples taken in thirty-five fetuses and newborns with gestational ages ranging between 16 and 41 weeks. Histomorphometric parameters were evaluated from frontal cuts in femurs, which were divided in several regions of interest of 0.56 mm^2. The data were organized so that parameters could be evaluated as a function of their distance to the metaphysis growth cartilage junction. Derived histomorphometric parameters such as recalled in section II.2 were computed. Parameters of bone formation (osteoid surface, osteoid thickness, osteoid volume), as well as parameters of bone resorption were also reported. Some parameters from this study useful to the scope of this paper are reproduced in Table I. Osteoid thickness and partial bone volume (BV/TV) increased with gestional age. The increase of BV/TV between 20 and 40%, was due to an increase of the mean trabecular thickness evaluated to 71 µm in the first period (16-27 weeks) and 93 µm in the last period of gestation (34-41 weeks). Interestingly there was a spatial evolution between partial bone volume, trabecular thickness, trabecular number, and cartilage volume with the distance to the growth plate. Partial bone volume and trabecular thickness were found to increase respectively of about 10% and 100% whereas trabecular number, and cartilage volume decreased. From the variation of trabecular thickness within the femoral metaphysis, the authors estimated the dynamics of trabecular thickening to about 3 µm/day. Indices of bone resorption decreased with gestional age, and were found to decrease with the distance from the growth plate. The authors emphasized that the changes involved for the femoral metaphyseal cancellous bone development were related to modeling.

Table I - Histomorphometric parameters in femoral metaphysis (from Salle et al. (25)).

	16-27 weeks	28-33 weeks	34-41 weeks
Gestational Age	20.5 ± 3.4	29.2 ± 1.7	38.1± 2.3
BV/TV (%)	24.0 ± 4.5	32.2 ± 6.3	33.6 ± 5.1
Tb.Th (µm)	71 ± 14	98 ± 15	93 ± 9
Tb.N (/mm)	3.4 ± 0.4	3.3 ± 0.5	3.6 ± 0.4

Results from 3D micro-CT

Vertebral bodies

The only study, to our knowledge, related to the three-dimensional evaluation of bone microarchitecture in fetal bone was reported in one of our previous works (31). The microarchitecture in vertebral body was evaluated by using 3D SR micro-CT at the ESRF (European Synchrotron Radiation Facility). Twenty-two lumbar vertebral bodies from preterm human stillborns with gestational age ranging between 16 to 26 weeks were studied. Cubic bone samples with a side of 7 and 2 mm were cut, embedded in methylmetacrylate and imaged using SR micro-CT. The samples were imaged both with a pixel size on the detector of 10.13 µm and 1.8 µm. The highest spatial resolution required to image the samples with a smaller transverse section (diameter < 2 mm) to avoid local tomography. The x-ray beam was monochromatic with an energy of 20 keV.

A 2D slice and a 3D display of the image of a vertebra sample (23 weeks) at the 10 µm scale are illustrated in Figure 2. The 2D slice in Figure 2, left, has a thickness of 10 µm and is similar to what may be seen in histology textbooks. When observed in three-dimensional space (Figure 2, right), a dense and isotropic 3D structure, with a peripheral part made of very thin bone struts, is clearly seen. These bone struts are not well rendered in these images, and were accurately studied in the images acquired at higher spatial resolution (voxel size 1.8 µm). Figure 3, left, illustrates a slice in the 3D micro-CT image acquired at the 2 µm scale. On the left side of this section, the small struts are well resolved, and on the right side, osteocyte lacunae may be observed in the bone structure. These observations were confirmed by comparing the micro-CT image to an histological slice. For this purpose, a 8 µm-thick section of the sample was stained with solochrome cyanin R and observed under light microscopy. The histological image matched with the micro-CT slice is presented in Figure 3 right (magnification 2). It shows organic tissue (cartilage) in pink, mineral tissue in blue, and calcified cartilage in light blue. At higher magnification, a high density of irregular osteocyte lacunae generally related to immature bone was observed. The examination of the histological slice under polarized light did not exhibit the presence of lamellar bone.

Quantitative morphologic parameters were then computed from volumes of interest (VOIs) extracted from the 3D images. The 10 µm scale was used to quantify the inner region as seen in the center of Figure 2, and the 2 µm scale for the quantification of the peripheral region. The main results are recalled in Table II. Partial bone volume, BV/TV, ranged between 30% and 55%, and a significant increase with gestational age was found. The mean trabecular thickness, in the inner region was around 100 µm, and no significant variation with aging in 16-26 weeks period was found. In the peripheral region, the bone

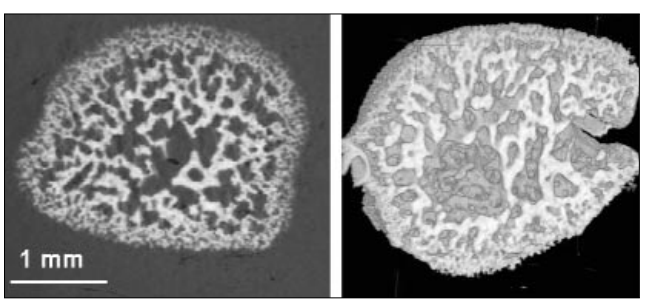

Figure 2 - Micro-CT image (voxel size: 10 µm) of cancellous bone in the vertebral body of a human fetus (GA = 23 weeks). Left: 2D slice (thickness = 10 µm), right: 3D display.

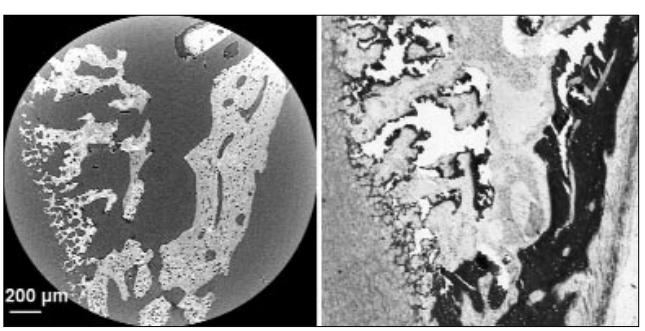

Figure 3 - Left: 2D slice of a micro-CT image (voxel size: 1.8 µm) of cancellous bone in the vertebral body of a human fetus (GA = 19 weeks), right: corresponding histologic section stained with solochrome cyanin R. The same features may be recognized.

Table II - 3D morphometric parameters in vertebral bodies (from Nuzzo et al., 27).

	Internal Bone Region			External Bone Region	
	BV/TV (%)	TbTh* (µm)	TbSp* (µm)	TbTh* (µm)	TbSp* (µm)
Min/Max	29.8 / 54	84.2 / 118.2	155.2 / 321.2	9.47 / 9.82	23.3 / 29.9
Mean (Std)	40.1 (10.1)	102.3 (11.3)	224.5 (63.8)	9.64 (1.17)	25.8 (3.1)

thickness was around 9 µm, corresponding to forming trabeculae. The presence of crystalline form of HAP was also assessed by synchrotron radiation diffraction. The size of crystal was found to increase significantly with gestational age.

Femoral metaphysis

We present here additional unpublished results obtained on fetal femoral metaphysis. Three femurs of respective gestational age (17, 20 and 29 weeks) were obtained from the same fetuses as discussed in the previous section. They were embedded in methylmetacrylate and imaged with 3D SR micro-CT at an energy of 20 keV, and a voxel size of 10 µm. The upper limit of each reconstructed volume was chosen at the frontier between mineralized tissue bone and cartilage, the later having little contrast. Smaller VOIs avoiding periostal bone, with a total height between 2.5 and 4.5 mm, were selected in the cancellous bone region to get quantitative parameters of trabecular microarchitecture.

Figure 4 illustrates a 2D transverse slice and a 3D display of the three femoral images. The 2D slices were taken at 3 mm below the top of the volumes. The 3D displays were made on the half 3D image to show the core of femurs. The 2D slices show the anisotropic elliptic shape of the sections perpendicular to the main direction of the femurs, with a large axis approximately 1,6 times larger than the small axis length. We may also note an increase of this length between 17 and 29 weeks (2.3 and 4.4 mm, respectively). The 3D displays clearly show the increase in size of the section as it goes towards the growth plate. The top of the 3D images corresponds to the cartilaginous epiphysis of the femur, which has little contrast in x-ray attenuation. Close to this region, bone trabeculae are very small, irregular, and less mineralized. Cancellous bone may clearly be seen either on the transverse sections as well as in the 3D rendering. From a visual point of view, trabeculae appear thinner in the region close to the growth plate.

The periostal region exhibits an irregular microstructure. This is illustrated in Figure 5 showing images selected from the 20-weeks femur. The image on left side shows a transverse slice cut at 8 mm from the top of the femur, and on the right side, a 3D display of a subvolume below this slice (height 2 mm). Concentric and parallel bone plates surround trabecular bone. This

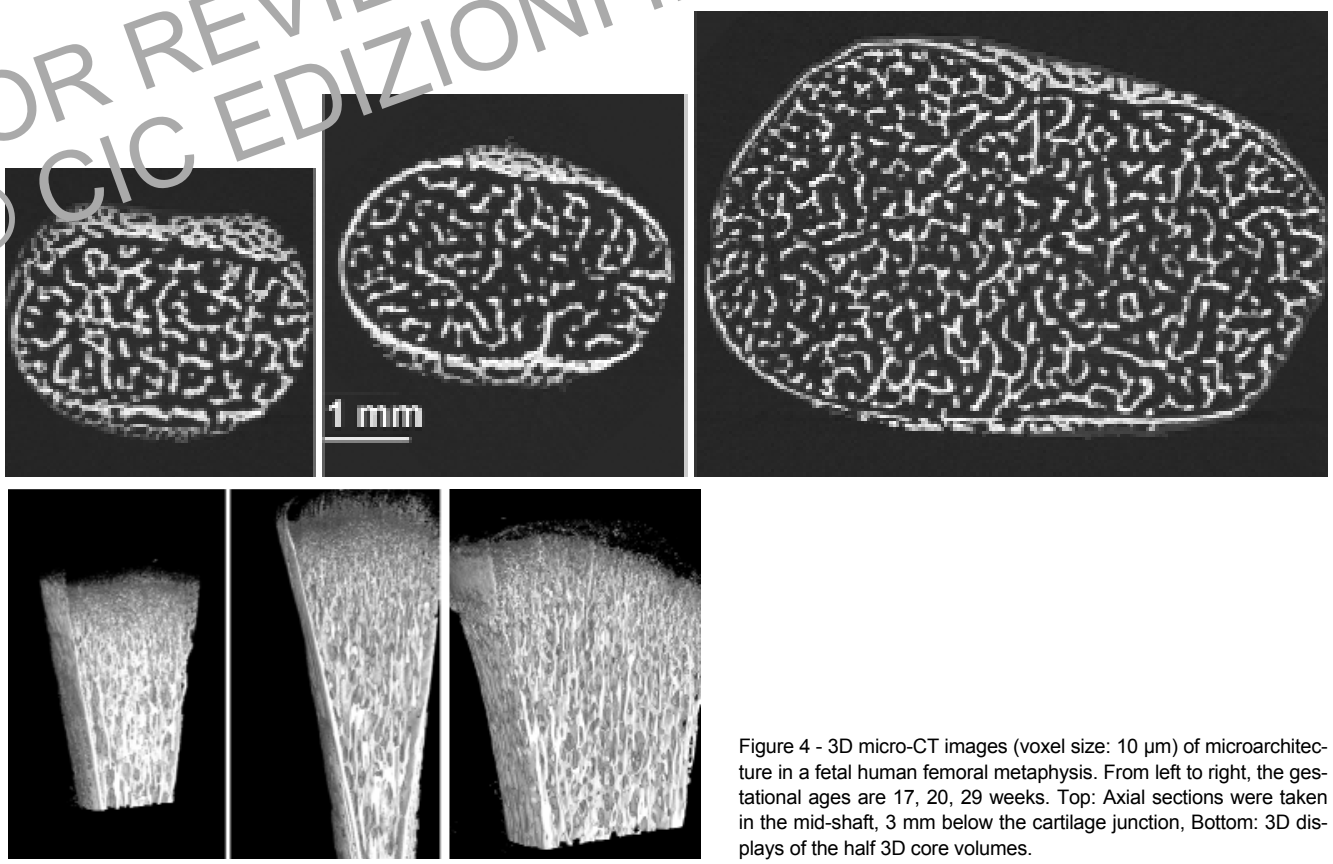

Figure 4 - 3D micro-CT images (voxel size: 10 µm) of microarchitecture in a fetal human femoral metaphysis. From left to right, the gestational ages are 17, 20, 29 weeks. Top: Axial sections were taken in the mid-shaft, 3 mm below the cartilage junction, Bottom: 3D displays of the half 3D core volumes.

Table III - 3D quantitative parameters measured in the femoral metaphysis of three human fetus (gestational ages 17, 20, 29 weeks) from 3D synchrotron radiation micro-CT images.

	Gestational age	17 weeks	20 weeks	29 weeks
Morphometric parameters	BV/TV (%)	23.53	22.19	22.28
	BS/BV (mm^{-1})	38.73	35.32	34.49
	Tb.N	4.77	3.62	3.76
	Tb.Sp (µm)	158.14	219.87	208.32
	Tb.Th (µm)	51.64	56.62	57.99
	Tb.Th* (µm)	70.11	82.28	81.49
Anisotropy parameters	DA	2.02	2.07	2.28
	Orientation	ZX	ZX	ZX
Geometric parameters	NV/BV (%)	7.53%	2.15%	2.68%
	PV/BV (%)	29.72%	27.68%	34.50%
	RV/BV (%)	62.74%	70.16%	62.82%
Connectivity parameter	Euler density (mm^{-3})	-112.52	-54.29	-64.83
Mineralization	Mean (g/cm^3)	0.827	0.839	0.803
	Coefficient of variation (%)	18	17	20

external shell may be interpreted as a primitive compacta which is described as irregular, multilayered and trabeculated due to remodeling (1). Note that at this stage the Haversian system is not yet in place. When looked closely, a large number of perforations may be seen in trabeculae. The images may also be used to evaluate the local degree of mineralization of bone. Brighter lines, corresponding to mineralization fronts, may be seen at the center of most bone structures. This is illustrated in the left image of Figure 5 and median lines may be observed in most bone slices. Due to the monochromaticity of the x-ray beam, the 3D image obtained in SR micro-CT reflects the map of the linear attenuation coefficient within the sample. Brighter gray levels correspond to higher mineral concentrations, and thus more ancient bone. Thus the images indicate that after initial bone deposition, bone expands symmetrically around this initial deposition, and at the same time the mineral content of the initial bone deposition increases. The external rings of bone in the periostal apposition region is in a less mineralized state (see Figure 5, left). The mean degree of mineralization of bone and its standard deviation, expressed in g/cm^3, were computed on the entire volumes using the method described in (27), and are reported in Table III.

Quantitative analysis was performed on cancellous bone VOIs using customized implementations of the different methods described. All parameters are summarized in Table III. The architectural parameters Tb.N, Tb.Th, Tb.Sp were derived using the 3D version of the MIL method. The mean derived-trabecular thickness in each sample was found between 52 and 58 µm. The main trabecular orientation as well as the degree of anisotropy were also evaluated from the MIL method. All samples were found to have a strong anisotropy and the main trabecular orientation was in the longitudinal direction. The second and third orientations were mainly equivalent showing some isotropy in the transverse slices. The discrete thickness map was used to compute the model-independent trabecular thickness Tb.Th* averaged on each VOI, found between 70 and 82 µm.

In addition, since the thickness map is by definition a 3D map of local thickness, it was possible to evaluate the mean model-independent thickness on each slice of the VOIs, and thus to follow the trabecular thickness as a function of the slice level. Similarly, the trabecular bone volume BV/TV was tracked in each slice. Since the main orientation of the sample was in the longitudinal direction, these evolutions may be expressed as a distance to the cartilage junction with a step equal to the slice thickness, i.e. 10 µm. A precise identification of the growth plate is difficult since x-ray attenuation only displays mineralized tissue. We observed on all samples an increase of trabecular bone volume and trabecular thickness with the distance to cartilage junction. Figure 6 illustrates these evolution on the 20-week sample. This quantitative behavior confirms the visual appearance of trabeculae in 3D displays (see Figure 4) showing the smallest trabeculae close to the cartilage junction. The changes in trabecular thickness as a function of distance d was well fitted by a linear regression (R^2=0.93, p<0,0001). However the increase slows slightly down when d is above 4.5 mm. If the linear regression is limited to the range [2-4.5 mm], the prediction is improved (R2=0.98, p<0,0001) and given by Tb.Th* = 15.03 d + 24.84. The trabecular thickness and trabecular bone volume as a function of the slice level are also significantly correlated (p<0,0001) but the variation of the trabecular bone volume shows some irregularities. This is explained by the fact that, if trabeculae are characterized by a specific thickness at a given level, the arrangement of bone volume is pseudo-periodic and thus bone mass varies from one slice to another.

The connectivity was evaluated by measuring the Euler density in mm^{-3}, i.e. the Euler number normalized by the analyzed VOI. Large negative numbers indicate a high degree of connectivity.

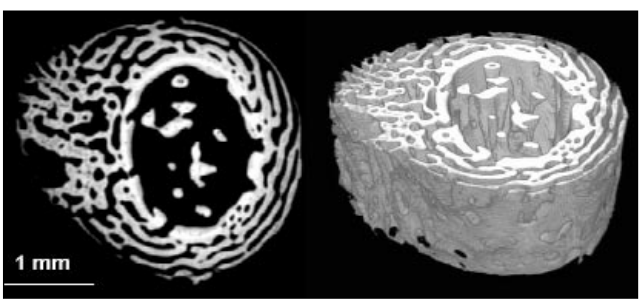

Figure 5 - 3D microstructure in femoral diaphysis in a human fetus (gestational age: 20 weeks). Left: transverse section showing periostal apposition, right: 3D display below this section (height: 2 mm).

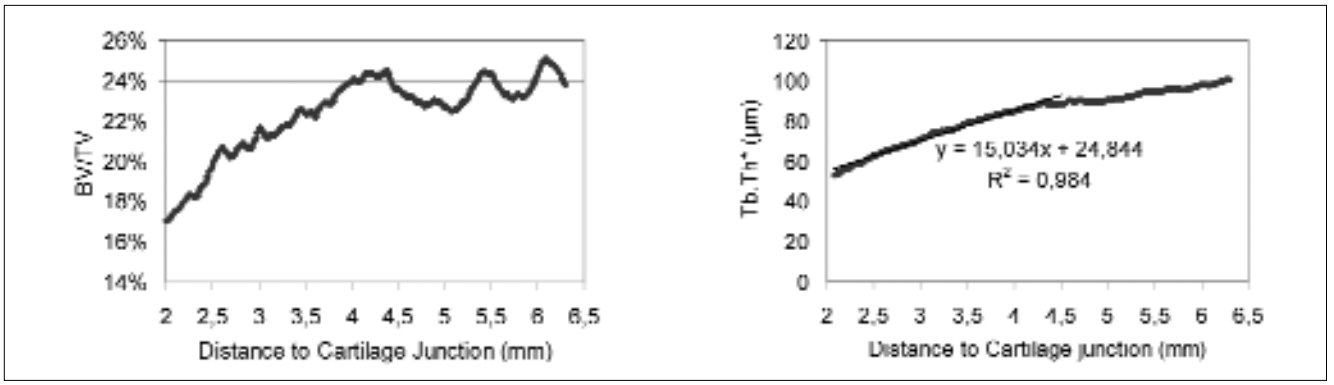

Figure 6 - Evolution of trabecular bone volume and trabecular thickness measured on the 3D image, as a function of distance to cartilage junction (29

Finally, our new geometric method described in section II.2 was used in order to identify the proportion of plates and rods in the structure. The results showed a strong prevalence of rod volume, between 62 and 70% as compared to plate volume around 30%, in each of the analyzed VOIs (see Table III). The examination of the local map shows that regions closest to the growth plate are mainly rodlike.

Discussion

The morphometric parameters obtained on fetal vertebrae and femurs evidenced a dense trabecular structure as compared to that of young adults. The histomorphometric analysis of femoral metaphysis and the 3D micro-CT analysis of vertebral bodies were consistent and showed a significant increase of trabecular bone volume BVTV with gestational age.

Three-dimensional analysis of anisotropy of cancellous bone in vertebra and in femoral metaphysis did not exhibit the same behavior at these two bone sites. The isotropy of trabecular bone in vertebral bodies demonstrated a growth that expands radially, while the anisotropy of the femoral metaphysis was related to the growth of long bone which spreads out longitudinally.

In the vertebral body, cancellous bone was characterized by an inner core made of trabeculae about 100 µm in thickness, and a peripheral layer with thinner trabeculae of about 9 µm. The peripheral region is supposed to correspond to newly formed bone struts which allows the vertebral body to expand radially. In the inner core, trabecular thickness is of the same order of magnitude than in adults.

In the femoral sample, the trabecular thickness provided by histomorphometry, was around 95 µm from the 28th week of gestation. In the new data presented here, we found a slightly smaller trabecular thickness of about 82 µm in the samples of 20 and 29 weeks. The trabecular thickness given here was averaged on a whole 3D volume starting close to the growth plate where trabeculae were the thinnest. Thus, the differences are expected to come mainly from differences in the location of the analyzed regions. The evolution of the trabecular thickness with the distance to cartilage junction observed from 3D micro-CT data are in agreement with the previous observation made in histomorphometry (25). Three-dimensional analysis allowed to follow this evolution with a distance step of 10 µm (slice thickness), and the data were very well fitted by a linear regression. In the 29-week sample, where the height of cancellous bone region analyzed was 4.5 mm, the trabecular thickness varied between 44 and 100 µm. The values are thus in the same range than that given in (25). Note that it is probable that the trabecular thickness reaches a plateau around 100-150 µm at some level (about 10 mm from the growth plate). By following the same line than in (25) and making the hypothesis that the growth plate advances at a rate of 0.16 mm/day, the slope of the linear regression for a distance to the growth plate between 2 and 4.5 mm, allows to estimate the thickening rate of trabeculae. Our measurements yield a thickening rate of 15,03 x 0,16 ~ 2,4 µm/day on the 29-week sample, 4 µm/day on the 17-week sample and 2.4 µm /day on the 20-week sample, thus a mean value close to the 3 µm/day found in (25). If our study is very limited in terms of the number of samples, the estimation of the slope in each sample is quite reliable since the distance step was 10 µm instead of the larger bandwidth (750 µm) due the method used in histomorphometry.

3D micro-CT also yielded new information on connectivity and geometry of bone structure. Connectivity was assessed via the Euler density which average on the 3 samples was -77.1/mm^3. Note that this value is very high as compared to that reported in studies dealing with adult bone closest to -5/mm^3 (41, 42). Thus, cancellous fetal bone appears to be highly connected. Connectivity density varies as the opposite of Euler density, and is increased either with the number of loops and/or with the perforations in plates. We hypothesize that this very high connectivity could be partly related to the high degree of vascularization of growing bone, plate perforation offering pathways for blood supply. To our knowledge, there are no comparative data in the literature concerning connectivity in bone development. Regarding the geometrical information on bone structure, a significant prevalence of rodlike trabeculae was found, which differed from the assumed usual platelike model of cancellous bone. This finding concerning the geometry of bone structure perfectly explains the differences in trabecular thickness estimated using the model assumption (Tb.Th) and the model independent method (Tb.Th*) as seen in Table 3. In this situation, the model-based trabecular thickness is typically underestimated (42). This new method could be used to follow the geometrical characteristics on cancellous bone at birth and in growing children, which are not fully elucidated.

Despite morphological information, the quantitative nature of 3D SR micro-CT enabled to estimate the distribution of the degree of mineralization within the 3D bone sample. The mean degree of mineralization in the examined samples was 0.823 g/cm^3, which is relatively low as compared to normal adults (27, 43). In addition, the images themselves allows to identify newly formed *versus* more ancient bone, typically found in the medial line of trabecular structure, and reflecting the thickening of trabeculae by bone apposition.

SR micro-CT is a three-dimensional imaging technique available at various scales. The 10 µm scale is appropriate for the accurate quantification of bone microarchitecture, even in fetal bone. The added value of 3D imaging as compared to histomorphometry is the availability of model independent parameters, anisotropy, connectivity and geometry characteristics. The

analysis of micro-CT images clearly showed that the typical parallel plate model was not appropriate at this stage of formation since the structure appeared made as a mixture of rods and plates, with a preponderance of rods. At a 2 µm scale, micro-CT images of femurs enable quantifying very thin struts as those that appeared in developing fetal vertebral bone. Other information such as for instance the analysis of lacunae would also be possible, but has still not be reported. The very good matching between micro-CT at 2 µm and histology demonstrates that for the analysis of mineralized tissue, micro-CT is as reliable as histology and even more since it avoids any deterioration due to slicing. However micro-CT only reflects mineralized tissue, cartilage may be guessed but with very little contrast, and does not allow to differentiate woven or lamellar bone.

We have reported a limited number of quantitative microarchitectural data obtained on fetal bones during their development. More studies are still required to get a better knowledge on the morphological mechanisms involved in bone growth.

Acknowledgment

We acknowledge Stefania Nuzzo for her participation to image acquisition and the ID19 group of the ESRF for help during experiment. We also acknowledge Dr R. Bouvier and Dr F. Dijoud, Depts of Pathology, Hospital E. Herriot & Hospital Debrousse - Lyon, for the bone samples. This work was done in the framework of the french GDR Stic-Santé (CNRS-Inserm 2647).

References

1. Gardner E. Osteogenesis in the human embryo and the fetus. In: Bourne GH, 2nd Ed., The biochemistry and the physiology of bone, London Academic. 1971;3:77-118.
2. Martini FH. Fundamentals of anatomy and physiology, Prentice Hall, 5th Ed, 2001.
3. Gray H, Williams PL, et al. Gray's anatomy: the anatomical basis of medicine and surgery. 38th Ed., Edinburgh, New York: Churchill Livingstone, 1995.
4. Noback CR, Robertson GG. Sequence of appearance of ossification centers in human skeleton during the first five prenatal months. Am J Anat. 1951;89:1-28.
5. Parfitt, AM. Quantum concept of bone remodelling and turnover: implications for the pathogenesis of osteoporosis. Calcif. Tissue Int. 1979;28:1-5.
6. Frost HM. Bone remodelling and its relation to metabolic bone diseases, C. Thomas, Springfield, IL, 1973.
7. Burr, DB, Martin RB. Errors in bone remodelling: Toward a unified theory of metabolic bone disease. Am J Anat. 1989;186:186-216.
8. Ben Hur H, Ornoy A. Ultrastructural studies of initial stages of mineralization of long bones and vertebrae in human fetuses, Acta Anat (Basel). 1984;119(1):33-39.
9. Oyedepo AC, Henshaw DL. Calcification of the lumbar vertebrae during human fetal development. Calcif Tissue Int. 1997;61(3): 179-82.
10. Burnell JM, Teubner EJ, Miller AG. Normal maturational changes in bone matrix, mineral, and crystal size in the rat. Calcif Tissue Int. 1980;31(1):13-9.
11. Grynpas MD, Tenenbaum HC, Holmyard DP. The emergence and maturation of the first apatite crystals in an in vitro bone formation system. Connect Tissue Res. 1989;21(1-4):227-33; discussion 234-7.
12. Rey C, Kim HM, Gerstenfeld L, et al. Characterization of the apatite crystals of bone and their maturation in osteoblast cell culture: comparison with native bone crystals. Connect Tissue Res. 1996;35:343-349.
13. Kuhn LT, Wu Y, Rey C, et al. Structure composition and maturation of newly deposited Calcium-phosphate crystals in chicken osteoblast cell cultures. J Bone Miner Res. 2000; 15:1301-1309.
14. Bagnall KM, Harris PF, Jones PRM. A radiographic study of the human fetal spine, 2. The sequence of development of ossification centres in the vertebral column. J Anat. 1977;124:791-802.
15. Bareggi R, Grill V, Sandreucci MA, et al. Development pathways of vertebral centra and neural arches in human embryos and fetuses. Anat Embryol. 1993;187:139-144.
16. Panattoni GL, Sciolla A, Isaia GC. Densitometric studies of developing vertebral bodies. Calcif Tissue Int. 1995 ;57:74-77.
17. Braillon PM, Salle BL, Brunet J, et al. Dual energy X-ray absorptiometry measurement of bone mineral content in newborns: validation of the technique. Pediatr Res. 1992;32:77-80.
18. Braillon PM, Lapillonne A, Ho PS, et al. Assessment of the bone mineral density in the lumbar vertebrae of newborns by quantitative computed tomography. Skeletal Radiology. 1996;25:711-715.
19. Filly RA, Simpson GF, Lindowski G. Fetal spine morphology and maturation during the second trimester: sonographic evaluation. J Ultrasound Med. 1987;6:631-637.
20. Budorick NE, Pretorius DH, Grafe MR, et al. Ossification of the fetal spine. Radiology. 1991;181:561-565.
21. Wallny TA, Schild RL, Fimmers R, et al. The fetal spinal canal: a three-dimensional study. Ultrasound Med Biol. 1999;25:1329-33.
22. Chitty LS, Altman DG, Henderson A, et al. Charts of fetal size: 3. Abdominal measurements. Br J Obstet Gynaecol. 1994;101(2):125-131.
23. Doubilet PM, Benson CB. Improved prediction of gestational age in the late third trimester. J Ultrasound Med. 1993;12(11):647-653.
24. Beyers N, Esser M, Alheit B, et al. Static bone histomorphometry in preterm and term babies. Bone. 1994;15(1):1-4.
25. Salle BL, Rauch F, Travers R, et al. Human fetal bone development: histomorphometric evaluation of the proximal femoral metaphysis. Bone. 2002;30(6):823-828.
26. Glorieux FH, Salle BL, Travers R, et al. Dynamic histomorphometric evaluation of human fetal bone formation. Bone. 1991;12(6): 377-381.
27. Nuzzo S, Meneghini C, Braillon P, et al. Microarchitectural and physical changes during fetal growth in human vertebral bone. J Bone Miner Res. 2003;18(4):760-768.
28. Doschak MR, Cooper DM, Huculak CN, et al. Angiogenesis in the distal femoral chondroepiphysis of the rabbit during development of the secondary centre of ossification. Anat. 2003;203 (2):223-33
29. Salome M, Peyrin F, Cloetens P, et al. A synchrotron radiation microtomography system for the analysis of trabecular bone samples. Med Phys. 1999;26(10):2194-204.
30. Martin Badosa E, Amblard D, Nuzzo S, et al. Excised bone structures in mice: imaging at three-dimensional synchrotron radiation micro CT. Radiology. 2003;229(3):921-8.
31. Nuzzo S, Meneghini C, Braillon P, et al. Microarchitectural and physical changes during fetal growth in human vertebral bone. J Bone Miner Res. 2003;18(4):760-8.
32. Nuzzo S, Peyrin F, Cloetens P, et al. Quantification of the degree of mineralization of bone in three dimensions using synchrotron radiation microtomography. Med Phys. 2002;29(11):2672-81. 4.
33. Parfitt AM, Drezner MK, Glorieux FH et al. Bone histomorphometry: standardization of nomenclature, symbols, and units. Report of the ASBMR Histomorphometry Nomenclature Committee. J Bone Miner Res. 1987;2(6):595-610.
34. Parfitt AM, Mathews CHE, Villanueva AR et al. Relationships between surface, volume, and thickness of iliac trabecular bone in aging and in osteoporosis. Journal of Clinical Investigation, 1989; 72:1396-1409.
35. Hipp JA, Simmons CA. Method-based differences in the automated analysis of the threedimensional morphology of trabecular bone. J Bone Miner Res. 1997;12(6):942-947.
36. Hildebrand T, Rüegsegger P. A new method for the model-independent assessment of thickness in three-dimensional images. Journal of Microscopy, 1997;185:67-75.
37. Martin-Badosa E, Elmoutaouakkil A, Nuzzo S, et al. A method for the automatic characterization of bone architecture in 3D mice microtomographic images. Comput Med Imaging Graph. 2003;27(6): 447-58.
38. Borgefors G. Distance transformations in arbitrary dimensions. Computer Vision, Graphics and Image Processing. 1984;27:321-345.
39. Hildebrand T, Ruegsegger P. Quantification of Bone Microarchitecture with the Structure Model Index. Comput Methods Biomech Biomed Engin. 1997;1(1):15-23.
40. Bonnassie A, Peyrin F, Attali D. A new method for analysing local shape in threedimensional images based on model axis transformation. IEEE Trans on Systems, Man and Cybernetics. 2003;33 (4):700-705.
41. Hildebrand T, Laib A, Müller R, et al. Direct three-dimensional morphometric analysis of human cancellous bone: microstructural data from spine, femur, iliac crest, and calcaneus. J Bone Miner Res.

1999;14:1167-1174.
42. Follet H, Bruyere-Garnier K, Peyrin F, et al. Relationship between compressive properties of human os calcis cancellous bone and microarchitecture assessed from 2D and 3D synchrotron microtomography. Bone. 2005;36(2):340-351.
43. Boivin GY, Chavassieux PM, Santora AC, et al. Alendronate increases bone strength by increasing the mean degree of mineralization of bone tissue in osteoporotic women. Bone. 2000; 27(5):687-94.